Journal of Solid State Chemistry 184 (2011) 3014–3020

Contents lists available at SciVerse ScienceDirect

Journal of Solid State Chemistry

journal homepage: www.elsevier.com/locate/jssc

Structural and catalytic properties of lanthanide (La, Eu, Gd) doped ceria

W.Y. Hernández *, O.H. Laguna, M.A. Centeno, J.A. Odriozola

Instituto de Ciencia de Materiales de Sevilla, Centro Mixto Universidad de Sevilla-CSIC, Avda. Americo Vespucio 49, 41092 Seville, Spain

ARTICLE INFO

Article history:
Received 12 April 2011
Received in revised form
19 August 2011
Accepted 14 September 2011
Available online 17 September 2011

Keywords:
Doped ceria
Oxygen vacancies
CO-oxidation

ABSTRACT

$Ce_{0.9}M_{0.1}O_{2-\delta}$ mixed oxides (M=La, Eu and Gd) were synthesized by coprecipitation. Independent of the dopant cation, the obtained solids maintain the F-type crystalline structure, characteristic of CeO_2 (fluorite structure) without phase segregation. The ceria lattice expands depending on the ionic radii of the dopant cation, as indicated by X-ray diffraction studies. This effect also agrees with the observed shift of the F_{2g} Raman vibrational mode. The presence of the dopant cations in the ceria lattice increases the concentration of structural oxygen vacancies and the reducibility of the redox pair Ce^{4+}/Ce^{3+}. All synthesized materials show higher catalytic activity for the CO oxidation reaction than that of bare CeO_2, being Eu-doped solid the one with the best catalytic performances despite of its lower surface area.

1. Introduction

For many years CeO_2-based materials have been intensively investigated as catalysts, structural and electronic promoters of heterogeneous catalytic reactions, oxide-ion conducting solid electrolytes in electrochemical cells, phosphor/luminescence, and ultraviolet absorbers [1–3]. For some practical applications, dopants such as transition and non-transition metal ions, may be introduced into the CeO_2 lattice, increasing its temperature stability and ability to store and release oxygen [4–6]. Metallic cations with ionic radius and electronegativity close to those of cerium are thought to be the most appropriate modifiers of structural and chemical properties of ceria [7]. The similarity in the ionic radii is also the criterion to predict the formation of a solid solution. Thus, rare earth elements are a good choice. In fact, oxides of rare earth elements, which present paramagnetism and other excellent properties, have been widely used as structural or electronic promoters to improve the activity, selectivity and thermal stability of catalysts [8–12]. When doping with lanthanide cations (i.e. Gd^{3+}, La^{3+}, Y^{3+}, $Eu^{3+/2+}$, $Pr^{4+/3+}$, among others), an increase in the concentration of oxygen vacancies in the ceria structure is expected. This feature promotes the migration of oxygen ions through the lattice oxide and provides the material with high oxygen ion conductivity [11]. In addition, the presence of oxygen vacancies have been correlated with an increase in the catalytic performances of the solids, attributed to the direct interaction of the surface defects with the reactive gas phase [10,13–15]. In the case of the CO oxidation reaction, several works have reported the formation of reactive peroxide (O_2^{2-}) or superoxide (O_2^-) species from the interaction of gaseous O_2 with the surface oxygen vacancies [16,17]. For metal supported catalysts (i.e. Au or Pt supported on CeO_2 or TiO_2), the presence of these punctual defects on the metal oxide hierarchies the interaction of the metallic phase with the support surface, allowing a high dispersion and special dynamic interaction (electronic enrichment, redispersion process, etc.) [14,18–20].

Considering the solid state properties, the high solubility of the rare earth cations in the ceria structure can allow an elevated oxygen vacancy concentration without any phase segregation. This situation could be ideal to study alone the influence of the concentration of these punctual defects on the catalytic properties of the material. Of course, the chemical nature of the rare earth cation (i.e. the possibility to have several oxidation states, such as Pr or Eu) should be also considered.

In this way, and taking into account the established relationship between the oxygen vacancies concentration and the catalytic activity towards CO oxidation of $Ce_{1-x}Eu_xO_{2-x/2}$ solid solutions [10], the present work has been focussed on the influence of the nature of the rare earth dopant cation in the ceria structure. Thus, different rare earth oxides (Gd_2O_3, Eu_2O_3 and La_2O_3) were employed to dope a CeO_2 solid and the defective structures produced characterized by Raman spectroscopy and correlated with the catalytic activity of the materials in the CO oxidation reaction.

2. Experimental

2.1. Preparation of the samples

CeO_2/M_2O_3 mixed oxides (M=La, Eu and Gd) were prepared by coprecipitation [10]. The appropriate amounts of $Ce(NO_3)_3 \cdot 6H_2O$

* Corresponding author. Present address: Université de Lyon, Institut de Recherches sur la Catalyse et l'Environnement de Lyon, UMR 5256, CNRS, Université Claude Bernard Lyon 1, 2 Avenue A. Einstein, F-69626 Villeurbanne, France.
E-mail address: yesidhdz@hotmail.com (W.Y. Hernández).

0022-4596/$ - see front matter © 2011 Elsevier Inc. All rights reserved.
doi:10.1016/j.jssc.2011.09.018

(Alfa-Aesar 99.5%), $La(NO_3)_3 \cdot 6H_2O$ (Fluka $\geq 99.0\%$), $Eu(NO_3)_3 \cdot 6H_2O$ (Alfa Aesar 99.9%) or $Gd(NO_3)_3 \cdot 5H_2O$ (Aldrich 99.99%) were dissolved in distilled water to obtain a 0.1 M solution, in order to achieve a 10% M_2O_3 weight percentage (w/w) in CeO_2. Then, the cationic solutions were precipitated by addition of ammonium hydroxide (30% w/w), at room temperature under continuous stirring at pH 9. The precipitated gels were washed by filtration with distilled water and dried overnight at 100 °C. Finally, the samples were calcined at 300 °C for 2 h (10 °C/min). For comparative purposes, pure cerium oxide was prepared in a similar way.

The series of synthesized materials were named Ce_*M*, where *M* corresponds to the lanthanide cation used as dopant.

2.2. Characterization

BET specific surface areas were measured by nitrogen adsorption at liquid nitrogen temperature in a Micromeritics ASAP 2000 apparatus. Before analysis, the samples were degassed 2 h at 150 °C in vacuum.

The composition of the samples, expressed as CeO_2 and M_2O_3 contents, were determined by X-ray fluorescence spectrometry (XRF) in a Panalytical AXIOS PW4400 sequential spectrophotometer with a rhodium tube as the source of radiation.

X-ray diffraction (XRD) analysis was performed on a Siemens D 500 diffractometer. Diffraction patterns were recorded with Cu $K\alpha$ radiation (40 mA, 40 kV) over a 2θ-range of 20–80° and a position-sensitive detector using a step size of 0.01° and a step time of 7 s. The lattice parameters of the samples were calculated adjusting the refinement Rietveld (using the X'Pert Plus program to perform a refinement in "automatic" mode) to *Fm*3-*m* space group. The reflection from the (1 1 1) plane was used for the determination of the average crystallite size, *D*, calculated from the Scherrer equation.

Temperature programmed reduction (TPR) of the catalysts was carried out using 5% hydrogen in Ar at 50 mL min^{-1}. About 50 mg of catalyst was loaded in a U-shaped quartz reactor and heated from room temperature to 900 °C at 10 °C min^{-1}. The effluent gases were analyzed by means of a TCD detector. Hydrogen consumption was determined upon calibration of the system with CuO (Strem Chemicals, 99.999% Cu).

The Raman spectra were recorded in a dispersive Horiva Jobin Yvon LabRam HR800 Microscope, with a 20 mW He–Ne green laser (532.14 nm), without filter, and with a 600 g mm^{-1} grating. The microscope used a 50× objective and a confocal pinhole of 100 μm. The Raman spectrometer is calibrated using a silicon wafer.

2.3. Catalytic activity

The CO oxidation tests were carried out in a conventional continuous flow U-shaped glass reactor (7 mm inner diameter) under atmospheric pressure. The sample (80 mg, $100\ \mu m < \phi < 200\ \mu m$) was placed between glass wools. A thermocouple in contact with the sample assures the right measure of the temperature. The feed mixtures were prepared using mass flow controllers (Bronkhorst). The reaction products were followed by mass spectrometry, using a Balzers Thermostar benchtop mass spectrometer controlled by the software Balzers Quadstar 422 with capabilities for quantitative analysis. The light-off curves of CO oxidation (400 °C, 5 °C/min) were obtained with a mixture of 3.4%CO (Air Liquide, 99.997% pure, < 3 ppm H_2O) and 21% O_2 (Air Liquide, 99.999% pure, < 3 ppm H_2O) balanced by He (Air Liquide, 99.999% pure, < 3 ppm H_2O) at a total flow rate of 42 mL/min. The catalysts were pre-activated "in situ" for 1 h at 400 °C with a mixture of 21% O_2 in He at a flow of 30 mL/min and then stabilized at room temperature before the light-off curve started [21].

3. Results and discussion

3.1. Chemical analysis and surface area

The chemical composition and textural properties of the prepared solids are shown in Table 1. The weight percentage of the different rare earths oxides incorporated to the cerium oxide is very similar to the intended value.

Textural analysis of the solids evidences the increase in the surface area of the bare CeO_2 after doping with all used lanthanide cations, without modification of the pore volume. Several authors have reported the increase of the surface area of CeO_2 by doping with 4+ (i.e. Zr^{4+}) or 3+ (as La^{3+}, Tb^{3+} or Y^{3+}) cations [22–24]. This fact was attributed to the higher thermal stability of the material afforded by the presence of the dopant cations, which avoids the nanoparticles sinterization during the calcination step. In some cases, the increased thermal stability of the doped material have been related with the segregation of the dopant cation on the grain boundaries, making difficult the agglomeration or sinterization of the oxide particles when the temperature is raised [14,24].

The nitrogen adsorption–desorption isotherms of the samples are presented in Fig. 1. The isotherms are typical of a mesoporous structure (IV type isotherm with H1 and H2 hysteresis loops), probably due to pores generated by particles crossed by nearly cylindrical channels or made by aggregates (consolidated) or agglomerates (unconsolidated) of spheroidal particles [25,26]. The pores can have uniform size and shape (type H1) or nonuniform ones (type H2) [26]. Similar textural properties have been reported for CeO_2 and other rare earth oxides such as La_2O_3, synthesized by precipitation in basic media and/or thermal decomposition of the precursor salts [27,28]. Our prepared CeO_2, Ce_Eu(10) and Ce_Gd(10) solids show an hysteresis loop nearest to H1 type, while that presented by Ce_La(10) material is closer to H2 type. These observations can be correlated with the average pore diameter of the solids (Table 1), in such a way that the sample with the highest pore diameters presents a H1 hysteresis loop while those samples with smaller diameters show a H2 one.

The pore size distribution depends on the lanthanide cation added (Fig. 2). The Ce_Eu(10) and Ce_Gd(10) solids present a bimodal pore distribution, very similar to that observed in the bare CeO_2, but with a higher volume adsorbed into the smaller pores. On the other hand, Ce_La(10) sample shows a narrow pore size distribution centered around the smaller diameters (~37 Å). Similar results were reported for Ce–Zr solid solutions without any evident correlation with the structural modification of the material [29].

Table 1
Chemical composition, textural properties and size of the introduced dopant cation, of the studied solids.

Code	Composition (%w/w)		S_{BET} (m^2/g)	V_p (cm^3/g)	D_p (Å)	Size dopant cation (Å) [b]
	CeO_2	M_2O_3 [a]				
CeO_2	100	–	69	0.141	76	Ce^{4+}/Ce^{3+} (0.97/1.14)
Ce_La(10)	91.6	8.4	98	0.115	44	La^{3+} (1.16)
Ce_Eu(10)	92.2	7.8	84	0.143	62	Eu^{3+} (1.07)
Ce_Gd(10)	89.2	10.8	96	0.138	53	Gd^{3+} (1.05)

V_p = Pore volume, D_p = Pore diameter.

[a] *M* = La, Eu, Gd.

[b] Ionic radii of the M^{3+} cations (VIII coordination).

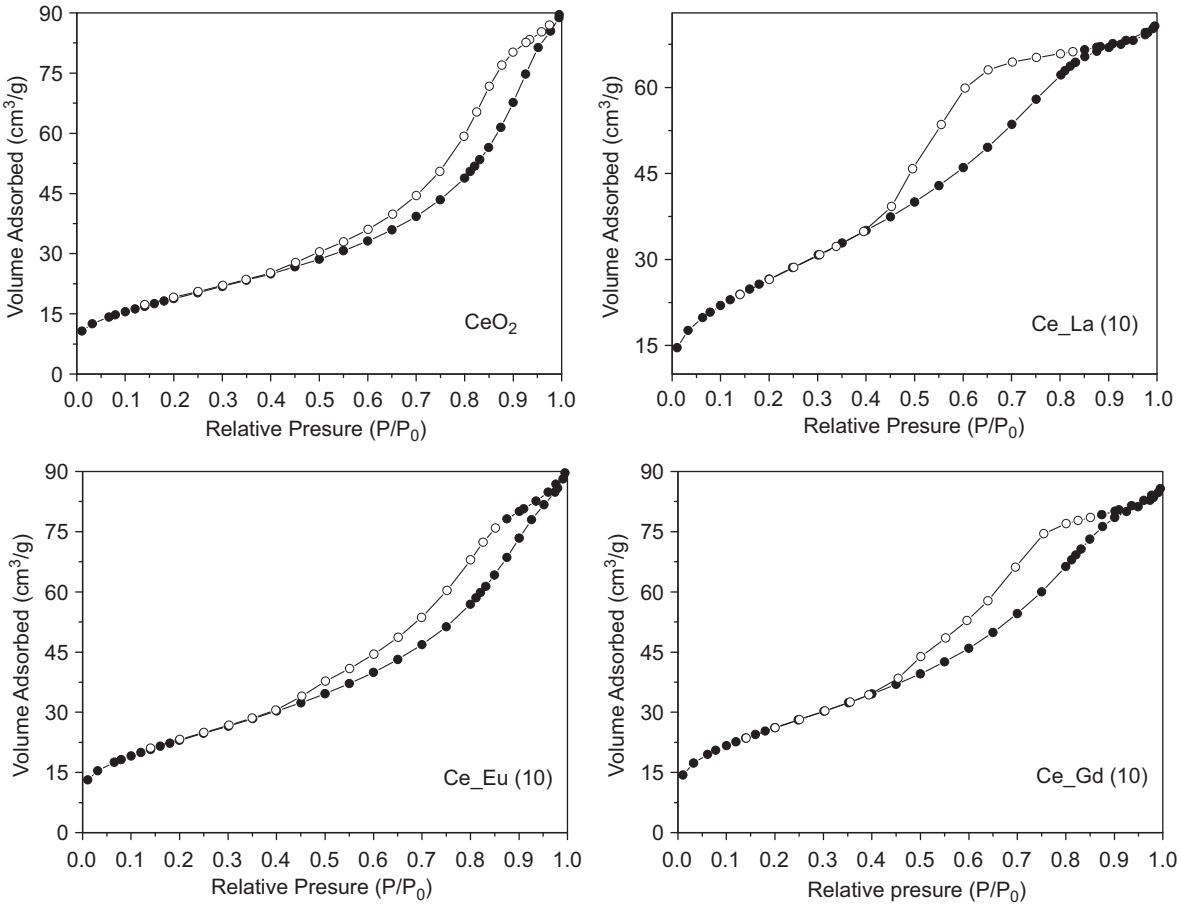

Fig. 1. N_2 absorption/desorption isothermal plots of the synthesized materials.

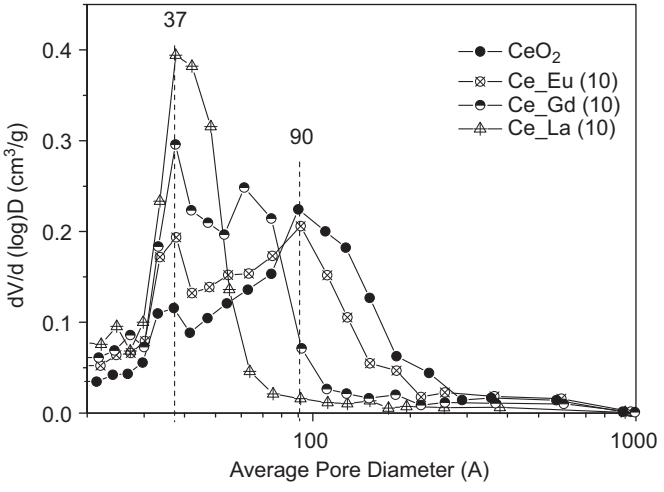

Fig. 2. Mesopore size distribution plots, obtained by BJH method for the prepared solids.

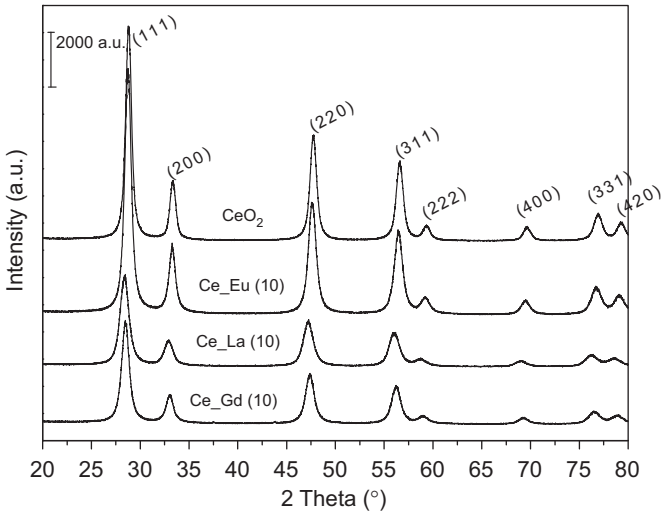

Fig. 3. X-ray diffraction patterns of the studied solids.

3.2. X-ray diffraction analysis (XRD)

In order to verify the formation of a Ce–*M* solid solution in the samples (type $Ce_{1-x}M_xO_{2-x/2}$ with M=La, Eu or Gd), a XRD study of the crystalline phases presented in the materials was carried out (Fig. 3). All materials maintain the F-type crystalline structure characteristic of CeO_2 (*Fm*-3*m* space group; JCPDS 43-1002). The absence of La_2O_3, Eu_2O_3 or Gd_2O_3 diffraction lines indicates the isomorphic substitution of Ce^{4+} by La^{3+}, Eu^{3+} or Gd^{3+} in the CeO_2 lattice and/or the existence of rare earth oxides highly dispersed on the surface of ceria.

Considering the XRD acquisition conditions employed in this work is very difficult to establish the substitution degree for each dopant cation in the ceria structure. For that purpose, a Rietveld analysis would be necessary. Nevertheless, the reflections observed in the XRD patterns for Ce_La(10) and Ce_Gd(10) solids are less intense and broader than those presented in the Ce_Eu(10) and CeO_2 ones. This result can be associated with a

less solubility of La^{3+} and Gd^{3+} in the host structure due to the different crystal structures (Hume–Rothery rules) of the ceria (face-centered cubic) in contrast to lanthana and gadolinia (hexagonal). In the case of europia, it presents a cubic structure as ceria, which favours the formation of the solid solution.

A shift towards lower 2θ values of the characteristic diffraction peaks of ceria is observed in all doped samples. The magnitude of the modification on the CeO_2 structure by the presence of the dopant cations was analyzed from the alteration in the lattice parameter and crystallite size of the mixed oxides. These results are presented in Table 2.

The lattice parameter of the samples increases linearly with the size of the introduced cation (Fig. 4). This result agrees with the substitution of Ce^{4+} by bigger M^{3+} cations (M=La^{3+}, Eu^{3+} and Gd^{3+}, Table 1) in the CeO_2 structure, which provokes the formation of a solid solution and the expansion of the oxide lattice.

In Table 2, a generalized decrease in the crystallite size of CeO_2 by the introduction of every dopant cation in the oxide structure is observed. This trend has been already reported for CeO_2 doped with trivalent cations and correlated with a retarding or stabilizing effect of the dopant element on the growth of the crystal oxide [22,23]. The decrease in the crystallite size of nanoparticulated CeO_2 has been also associated to surface energetic factors [10,30,31], due to microstrain effects provoked by the expansion of the lattice parameter caused by the presence of trivalent cations in the ceria structure.

3.3. H_2-TPR analysis

H_2 consumption profiles during the TPR experiments are plotted in Fig. 5. The temperatures of the peak maxima and their respective hydrogen consumption are given in Table 3. The TPR profile of pure ceria shows two main peaks at 414 °C (low temperature, LT peak) and 799 °C (high temperature, HT peak), which have been, respectively, attributed to the reduction of the surface and bulk ceria [32,33]. Additionally, with the LT peak, is possible to observe a shoulder at higher temperatures (Table 3), which can be associated with the surface heterogeneity of the sample. For the Ce_Gd(10), Ce_Eu(10) and Ce_La(10) samples, the temperature of the LT peak slightly shifts to higher temperatures compared to that of bare CeO_2, presenting also a higher hydrogen consumption (except for Ce_Gd(10) solid). This feature can be related with the structural modifications induced in the ceria lattice when some Ce^{4+} cations are substituted with Gd^{3+}, Eu^{3+} and La^{3+} cations. In this way, even the doped materials reduced at slightly higher temperature than pure CeO_2, the increase in the concentration of surface oxygen vacancies could promote the adsorption and dissociation of H_2, improving that way the surface and sub-surface reduction of the material together with higher hydrogen consumption [14]. On the other hand, in all the doped materials, the HT peak shifts to lower reduction temperatures and decreases in its hydrogen consumption compared to pure CeO_2 (Table 3). As can be expected, the presence of the dopant cations leads to a lower lattice strain and higher free volume in the oxide network, and then facilitates the equilibrium between surface and bulk oxygen atoms. The defects created during the incorporation of Gd^{3+}, Eu^{3+} and La^{3+} eases the formation of labile oxygen vacancies facilitating the relatively high mobility of bulk oxygen species within the lattice cell [34].

Among the prepared materials, Ce_Eu(10) solid presents the lowest temperature reduction processes (Table 3). As it has been recently established for this material, a high concentration of surface oxygen vacancies improves the adsorption and dissociation of H_2 from the gas phase as well as the surface and sub-surface reaction with it [14]. So, a higher concentration of these

Table 2
Crystallite size, phase analysis and lattice parameters of the synthesized materials.

Code	Crystallite size, *D* (nm)	Phase analysis [a]	Lattice parameter, *a* (Å)
CeO_2	15	*F*	5.4142
Ce_La(10)	11	*F*	5.4378
Ce_Eu(10)	13	*F*	5.4251
Ce_Gd(10)	11	*F*	5.4209

[a] F: F-type cubic.

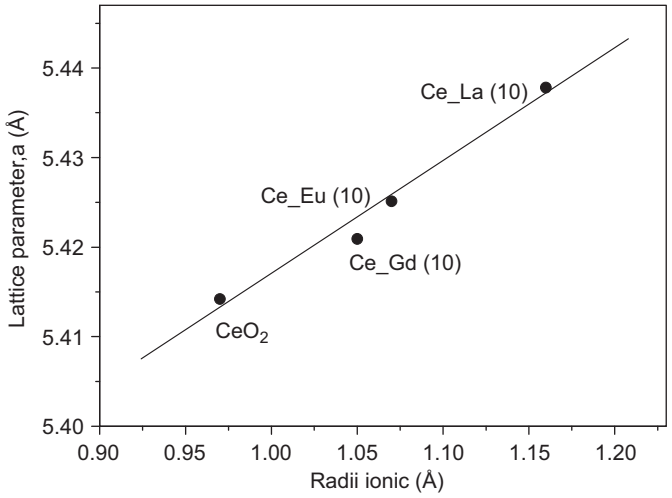

Fig. 4. Lattice parameters as a function of the ionic radii of the employed dopant cation.

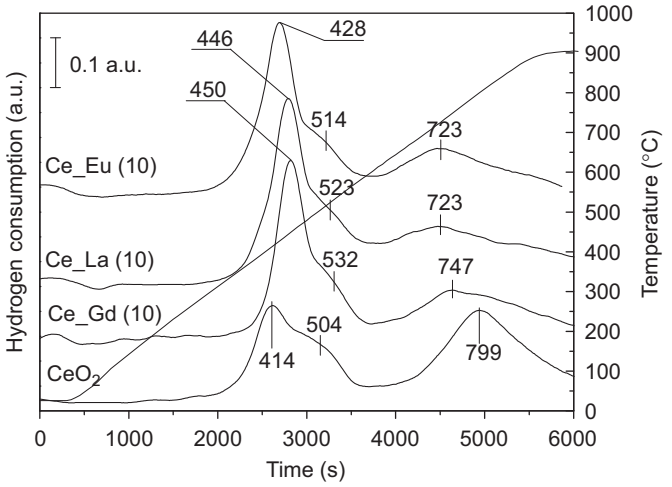

Fig. 5. H_2-TPR profiles of the studied solids.

Table 3
TPR peak maxima and H_2 uptake of synthesized solids.

Code	Peak position (°C)		H_2 consumption (μmol/g of CeO_2)	
	T_{LT}	T_{HT}	η_{LT}	η_{HT}
CeO_2	414; 504	799	571	428
Ce_La(10)	446; 523	723	870	513
Ce_Eu(10)	428; 514	723	766	495
Ce_Gd(10)	450; 532	747	706	491

surface punctual defects can be expected by doping the ceria structure with Eu^{3+} in comparison with La^{3+} and Gd^{3+}.

3.4. Raman spectroscopy

Crystals with the fluorite structure, space group $Fm\text{-}3m$ (O_h^5) have an exceptionally simple vibrational structure with one IR active phonon of T_{1u} symmetry and one Raman active phonon of F_{2g} symmetry at $k=O$ [35]. The first order Raman spectra of CeO_2 is characterized by the presence of a F_{2g} vibrational mode around 465 cm^{-1}, ascribed to the symmetric breathing mode of the oxygen atoms surrounding each Ce^{4+} cation [35–37]. Because this vibrational mode is only dependent of the oxygen movement, their peak characteristics (width and position) are extremely sensible to the disorder induced in the oxygen ion sublattice of the oxide.

Fig. 6 shows the Raman spectra obtained for the studied samples. Pure CeO_2 solid presents two main bands at 462 and 1050 cm^{-1}. The more intense one (465 cm^{-1}) corresponds to the F_{2g} vibrational mode described before. The comparative weak band at 1050 cm^{-1} can be due to the primary A_{1g} asymmetry, combined with small additional contributions from E_g and F_{2g} symmetries [31,38,39]. Besides this, two additional bands appear in the spectra of the doped solids at about 600 and 545 cm^{-1} for Ce_Gd(10) and Ce_La(10) solids, and 600 and 529 cm^{-1} for Ce_Eu(10) one. The signal at 600 cm^{-1} is much less pronounced in the pure CeO_2 solid, but its presence can be intuited in its Raman spectrum. In general, the presence of these Raman bands can be attributed to the existence of oxygen vacancies in the oxide structure [10,40,41]. This situation is expected taking into account the replacement of Ce^{4+} by M^{3+} cations in the structure of the solid, as was discussed before by XRD. Oxygen vacancies are produced in the oxygen sublattice to compensate the effective negative charge of the dopant cation introduced. Therefore, the doped CeO_2 generally losses the translational symmetry of the crystal, leading to the destruction of the wave vector $k=0$ selection rule for Raman scattering. Consequently, phonons at all parts in the Brillouin zone will contribute to the optical spectra [41].

From the analysis of the phonon–dispersion curves, employing the rigid-ion model, some authors have shown that the formation of punctual defects in the crystalline structure of doped CeO_2 provokes the broadening and shifting of the F_{2g} Raman mode, along with the emergence of new vibrational modes around 500–600 cm^{-1} [40,41]. In this way, the band at 600 cm^{-1} was assigned to the presence of intrinsic oxygen vacancies in ceria, due to their non-stoichiometric condition (presence of Ce^{3+} replacing Ce^{4+} in the lattice) [40,42]. On the other hand, the Raman bands around 545 cm^{-1} observed in Ce_Gd(10) and Ce_La(10) solids, and 529 cm^{-1} in Ce_Eu(10) one, can be assigned to the generation of oxygen vacancies by the insertion of the dopant cations in the ceria structure [40,42,43]. The presence of this band confirms the existence of the solid solution [39]. Because the intensity of the Raman band at 529 cm^{-1} in the Ce_Eu(10) solid is so much relevant in comparison with the equivalent signal in the other materials, a qualitatively higher concentration of oxygen vacancies can be deducted for the Eu-doped ceria. These results are in a good agreement with the data discussed by H_2-TPR analysis.

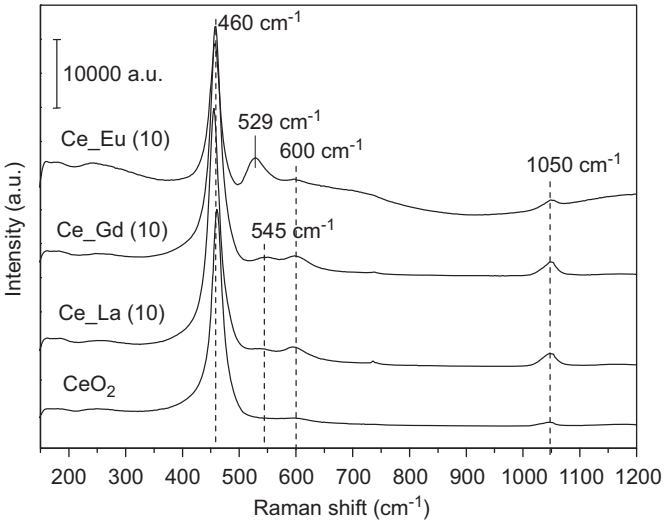

Fig. 6. Raman spectra of the studied materials.

The reason because the band at 600 cm^{-1} is less evident in the bare CeO_2 in comparison with the doped solids could be related with the differences in the crystallite size of the materials. By Raman analysis on nanocrystalline ceria (grain size ≤ 100 nm), Kosacki et al. [36] showed that the non-stoichiometry of the crystal can be controlled by its microstructure. In this sense, an increase in the defects concentration in CeO_2 was observed when the grain size decreases, and associated to a reduction in the enthalpy of formation of oxygen vacancies. In the same way, Tsunekawa et al. [30] correlated the expansion of the CeO_2 lattice parameter with a decrease in the crystal size of the nanoparticulated material. This effect was attributed to the Ce^{3+} surface enrichment concomitant to the increase in the surface to volume ratio on the nano-crystals, which also induces changes in the Raman spectrum of the material [31,44]. Hence, the lower crystallite size showed by the doped ceria compared to that of the pure one, could improve the Ce^{3+} surface concentration on the solids. Therefore, the non-stoichiometric condition of the oxide would be favored, and the appearance of the Raman band at 600 cm^{-1}, promoted.

The modifications of the F_{2g} mode observed in the Raman spectra of the synthesized materials were also analyzed. Doped CeO_2 materials present a shift of this vibrational mode to lower energies, in comparison with undoped CeO_2 solid (Fig. 6). Several factors can contribute to the changes in the Raman peak position and linewidth of the F_{2g} mode in the domain size of nanoparticles. These include phonon confinement, strain, broadening associated with the size distribution and variations in phonon relaxation with particle size. Changes in the lattice parameter can affect also the Raman peak position [31]. Employing a thermodynamic model to investigate the Raman frequency shifts of semiconductor nanocrystals, Yang et al. [45] found that the Raman frequency decreases as the nanocrystal size decreases. The Raman red shift was ascribed to the size-induced phonon confinement effect and surface relaxation. This condition results in the higher energetic state of the semiconductor surface atoms. As a consequence, the atomic vibrational amplitude increases as the crystal size decreases, decreasing that way the atomic vibrational frequency. For CeO_2 doped with rare earth metals, McBride et al. [40] established two different mechanisms able to contribute in the shift of the F_{2g} Raman band: (i) the increase in the concentration of oxygen vacancies and (ii) the expansion–contraction of the oxide lattice. Taking into account the (ii) effect, the changes in the Raman vibration frequency ($\Delta\omega$) produced by modifications in the lattice parameter of the crystal (Δa), may be described in terms of the Grüneisen parameter employing the equation

$$\Delta w = -3\gamma\omega_0\Delta a/a_0 \quad (1)$$

where ω_0 is the Raman frequency of the F_{2g} mode in un-doped CeO_2, a_0 their lattice parameter, and γ the Grüneisen constant which value can be considered as 1.24 [40].

Fig. 7 shows the relationship between the F_{2g} vibrational mode from the synthesized samples (measured and calculated by Eq. (1)) and the lattice parameter calculated by XRD analysis (Table 2).

Because changes in the lattice parameter, oxygen vacancies concentration and decrease of the particle size material may affect the F_{2g} Raman peak position in ceria related materials, the calculated Raman shift values are in a good agreement with the measured ones, considering only the modifications in the lattice parameter of the CeO_2. From this result is possible to correlate the effective incorporation of the dopant cation in the CeO_2 crystalline structure with the energy changes generated in the network of the material.

3.5. Catalytic activity. CO oxidation

Fig. 8 shows the CO conversion as a function of the temperature for the synthesized materials. All prepared solids were active in the CO oxidation reaction, increasing the CO conversion with temperature. CO abatement begins at about 300 °C reaching CO conversion values higher than 80% at 400 °C. In this temperature range, all doped materials always show higher conversions than those of the un-doped CeO_2 solid. Hence, in a general way, the presence of the rare earth cations in the CeO_2 structure promotes

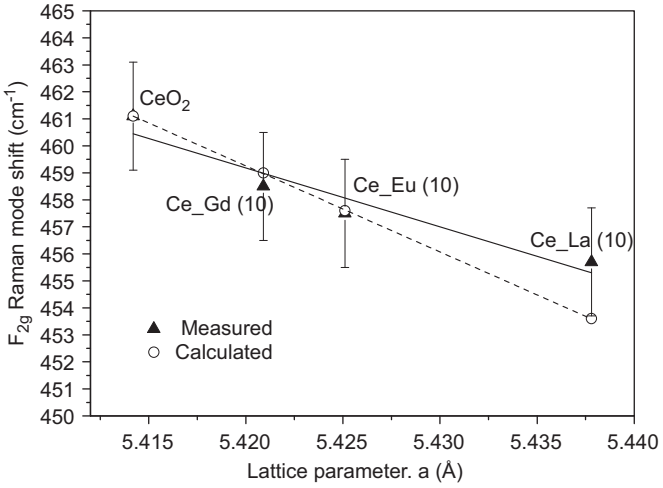

Fig. 7. F_{2g} Raman mode shift versus lattice parameter of the studied solids.

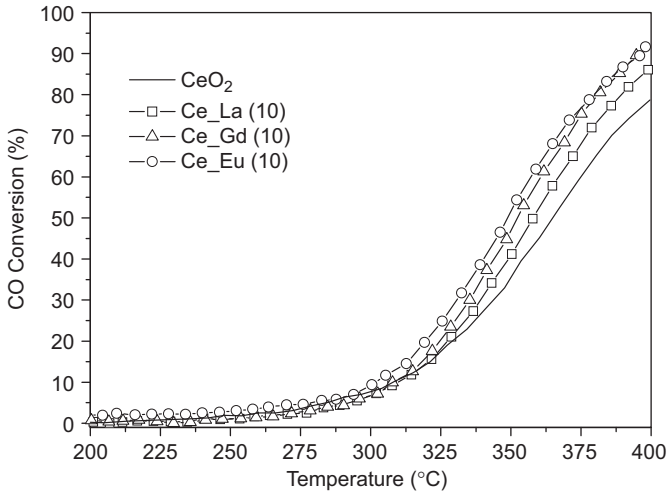

Fig. 8. CO conversion of the studied solids as a function of the temperature.

the catalytic performances towards CO oxidation of the oxide. Similar results have been reported when doping ceria with Zr^{4+} [46,47], La^{3+} [23,48], $Pr^{4+/3+}$ [39,49], Fe^{3+} [6,50,51] and Zn [52] cations, among others. In all these works, the higher catalytic activity of the materials was correlated with the increment in the concentration of oxygen vacancies in the solid solution. The CeO_2 modification with isovalent cations such as Zr^{4+}, improves the oxygen storage capacity (OSC) of the material, due to the decrease of the reduction energy of the Ce^{4+}/Ce^{3+} redox pair. As a result, the creation and diffusion of oxygen vacancies are improved, while increasing the solid thermal stability [53,54]. On the other hand, the doping of CeO_2 with aliovalent cations (M^{3+}), strongly improves the oxygen vacancies generation due to the effective negative charge compensation coming from the presence of the dopant in the ceria structure. Depending of the chemical nature of the introduced cation, these punctual defects can be delocalized (mobiles), or highly localized around the dopant cations [55,56].

The role of the oxygen vacancies in the CO oxidation reaction mechanism is still controversial. Some authors claimed that their main role is to provide active sites to the adsorption of molecular oxygen from the gas phase, facilitating the generation of reactive species such as peroxides (O_2^{2-}) or superoxides (O_2^-), being these species the responsible of the direct oxidation of the carbon monoxide [16,57,58]. In other works, the structural distortion in the ceria structure due to the presence of the dopant cation, have been proposed to facilitate the oxygen depletion from the surface material (lattice oxygen), enhancing their reactivity towards the CO adsorption [3,48,50,59]. In such mechanism, the relationship between the catalytic activity and the oxygen mobility can be associated to the nature of the dopant cation [60]. The type of conduction (ionic and/or electronic) characteristic of the material greatly influences the preferential mechanism during the reaction [61].

In all solids studied in this work, whatever the nature of the dopant cation introduced, the generation of structural defects in the CeO_2 material, and the enhancement of its catalytic activity in CO oxidation reaction is produced. Nevertheless, despite its lowest surface area (Table 1), Ce_Eu(10) solid shows a slightly higher catalytic activity in front of the others. This feature is evident from its smallest T_{50} value (temperature at which the 50% CO conversion is achieved, Table 4).

This result can be related with the high surface concentration of oxygen vacancies in the Ce_Eu(10) solid, as it has been already established by us in this type of materials [10,14]. In this way, although all dopants used in this work are able to increase the oxygen vacancies concentration in CeO_2, the presence of europium in the structure could promote the surface character of these punctual defects. Additionally, the Eu^{3+}/Eu^{2+} redox pair whose potential is close to 0 ($E^\circ = -0.36$) [62], could promote the formation and stabilization of oxygen vacancies for low Eu/Ce ratios [10], and increasing the ionic and electronic conductivity of the material.

Thus, Eu-doped ceria solid is shaping as a very interesting material to be used as catalytic support in oxidation reactions, taking into account two principal facts: (i) the active nature of the surface oxygen vacancies in oxidation process and (ii) the role of

Table 4
T_{50} value obtained for the studied solids in the CO oxidation reaction.

Code	T_{50} (°C)
CeO_2	366
Ce_La(10)	359
Ce_Gd(10)	354
Ce_Eu(10)	350

the oxygen vacancies in the dynamic interaction of the gas phase with metallic supported phases such as gold-nanoparticles [14].

4. Conclusions

The formation of $Ce_{1-x}M_xO_{2-x/2}$ solid solutions (M=La, Eu and Gd) was verified by XRD analysis and Raman spectroscopy for M_2O_3 contents around 10% (w/w). The insertion of the rare earth cations in the CeO_2 structure provokes an increase in the oxygen vacancies concentration of the material by two possible mechanisms: the first one, a direct replacement of Ce^{4+} by M^{3+} in the octahedral lattice positions in the oxide structure, and the second one, the promotion of the non-stoichiometric condition of the cerium oxide, by the reduction of Ce^{4+} to Ce^{3+}. The increase in the oxygen vacancies concentration has a positive influence on the catalytic activity of the solids towards CO oxidation, especially in the case of the Ce_Eu(10) solid.

Acknowledgment

The financial support for this work has been obtained from Junta de Andalucía (TEP106) and Spanish Ministerio de Ciencia e Innovación (ENE2009-14522-C05-01), cofinanced by FEDER funds from European Union. W. Y. Hernández thanks the AlBan program for the fellowship awarded (E06D101739CO).

References

[1] A. Trovarelli, Catalysis by Ceria and Related Materials, Imperial College, London, 2002.
[2] A. Trovarelli, Catal. Rev. 38 (1996) 439–520.
[3] A. Trovarelli, Comments Inorg. Chem. 20 (1999) 263–284.
[4] M.V. Ganduglia-Pirovano, A. Hofmann, J. Sauer, Surf. Sci. Rep. 62 (2007) 219–270.
[5] O.H. Laguna, F.R. Sarria, M.A. Centeno, J.A. Odriozola, J. Catal. 276 (2010) 360–370.
[6] O.H. Laguna, M.A. Centeno, G. Arzamendi, L.M. Gandia, F. Romero-Sarria, J.A. Odriozola, Catal. Today 157 (2010) 155–159.
[7] T.H. Etsell, S.N. Flengas, Chem. Rev. 70 (1970) 339 &.
[8] K. Krishna, A. Bueno-López, M. Makkee, J.A. Moulijn, Appl. Catal. B 75 (2007) 189–200.
[9] Z. Wang, Z. Quan, J. Lin, Inorg. Chem. 46 (2007) 5237–5242.
[10] W.Y. Hernández, M.A. Centeno, F. Romero-Sarria, J.A. Odriozola, J. Phys. Chem. C 113 (2009) 5629–5635.
[11] H. Yokokawa, T. Horita, N. Sakai, K. Yamaji, M.E. Brito, Y.P. Xiong, H. Kishimoto, Solid State Ionics 177 (2006) 1705–1714.
[12] Y.S. She, Q. Zheng, L. Li, Y.Y. Zhan, C.Q. Chen, Y.H. Zheng, X.Y. Lin, Int. J. Hydrogen Energy 34 (2009) 8929–8936.
[13] R.Q. Long, Y.P. Huang, H.L. Wan, J. Raman Spectrosc. 28 (1997) 29–32.
[14] W.Y. Hernández, F. Romero-Sarria, M.A. Centeno, J.A. Odriozola, J. Phys. Chem. C 114 (2010) 10857–10865.
[15] M. Daturi, N. Bion, J. Saussey, J.C. Lavalley, C. Hedouin, T. Seguelong, G. Blanchard, Phys. Chem. Chem. Phys. 3 (2001) 252–255.
[16] M.I. Domínguez, F. Romero-Sarria, M.A. Centeno, J.A. Odriozola, Appl. Catal. B 87 (2009) 245–251.
[17] J. Guzman, S. Carrettin, A. Corma, J. Am. Chem. Soc. 127 (2005) 3286–3287.
[18] M.G. Sanchez, J.L. Gazquez, J. Catal. 104 (1987) 120–135.
[19] N. Lopez, J.K. Norskov, Surf. Sci. 515 (2002) 175–186.
[20] F. Romero-Sarria, L.M.T. Martínez, M.A. Centeno, J.A. Odriozola, J. Phys. Chem. C 111 (2007) 14469–14475.
[21] M.I. Domínguez, M. Sánchez, M.A. Centeno, M. Montes, J.A. Odriozola, Appl. Catal. A 302 (2006) 96–103.
[22] F. Guodong, F. Changgen, Z. Zhao, J. Rare Earths 25 (2007) 42–47.
[23] A. Bueno-López, K. Krishna, M. Makkee, J.A. Moulijn, J. Catal. 230 (2005) 237–248.
[24] M. Li, Z. Liu, Y. Hu, M. Wang, H. Li, J.Rare Earths 26 (2008) 357–361.
[25] K.S.W. Sing, Reporting physisorption data for gas/solid systems. 1984, pp. 567–583.
[26] G. Leofanti, M. Padovan, G. Tozzola, B. Venturelli, Catal. Today 41 (1998) 207–219.
[27] J.L.G. Fierro, S. Mendioroz, A.M. Olivan, J. Colloid Interface Sci. 107 (1985) 60–69.
[28] J.L.G. Fierro, S. Mendioroz, A.M. Olivan, J. Colloid Interface Sci. 100 (1984) 303–310.
[29] M. Hirano, A. Suda, J. Am. Ceram. Soc. 86 (2003) 2209–2211.
[30] S. Tsunekawa, R. Sivamohan, S. Ito, A. Kasuya, T. Fukuda, Nanostructured Mater. 11 (1999) 141–147.
[31] J.E. Spanier, R.D. Robinson, F. Zhang, S.W. Chan, I.P. Herman, Phys. Rev. B 64 (2001) 2454071–2454078.
[32] L. Ilieva, G. Pantaleo, I. Ivanov, R. Zanella, A.M. Venezia, D. Andreeva, Int. J. Hydrogen Energy 34 (2009) 6505–6515.
[33] Q. Fu, A. Weber, M. Flytzani-Stephanopoulos, Catal. Lett. 77 (2001) 87–95.
[34] L. Katta, P. Sudarsanam, G. Thrimurthulu, B.M. Reddy, Appl. Catal. B 101 (2010) 101–108.
[35] V.G. Keramidas, W.B. White, J Chem. Phys. 59 (1973) 1561–1562.
[36] I. Kosacki, T. Suzuki, H.U. Anderson, P. Colomban, Solid State Ionics 149 (2002) 99–105.
[37] G. Gouadec, P. Colomban, Prog. Cryst. Growth Charact. Mater. 53 (2007) 1–56.
[38] W.H. Weber, K.C. Hass, J.R. McBride, Phys. Rev. B 48 (1993) 178–185.
[39] M.-F. Luo, Z.-L. Yan, L.-Y. Jin, J. Mol. Catal. A 260 (2006) 157–162.
[40] J.R. McBride, K.C. Hass, B.D. Poindexter, W.H. Weber, J. Appl. Phys. 76 (1994) 2435–2441.
[41] A. Nakajima, A. Yoshihara, M. Ishigame, Phys. Rev. B 50 (1994) 13297–13307.
[42] Z.D. Dohcevic-Mitrovic, M. Radovic, M. Šcepanovic, M. Grujic-Brojcin, Z.V. Popovic, B. Matovic, S. Boskovic, Appl. Phys. Lett. 91 (2007).
[43] Z.D. Dohcevic-Mitrovic, M.J. Scepanovic, M.U. Grujic-Brojcin, Z.V. Popovic, S.B. Boskovic, B.M. Matovic, M.V. Zinkevich, F. Aldinger, Solid State Commun. 137 (2006) 387–390.
[44] F. Zhang, S.W. Chan, J.E. Spanier, E. Apak, Q. Jin, R.D. Robinson, I.P. Herman, Appl. Phys. Lett. 80 (2002) 127.
[45] C.C. Yang, S. Li, J. Phys. Chem. B 112 (2008) 14193–14197.
[46] M. Nolan, J. Phys. Chem. C 113 (2009) 2425–2432.
[47] A. Varez, E. Garcia-Gonzalez, J. Jolly, J. Sanz, J. Eur. Ceram. Soc. 27 (2007) 3677–3682.
[48] I. Yeriskin, M. Nolan, J. Chem. Phys. 131 (2009).
[49] B.M. Reddy, G. Thrimurthulu, L. Katta, Y. Yamada, S.E. Park, J. Phys. Chem. C 113 (2009) 15882–15890.
[50] H. Bao, X. Chen, J. Fang, Z. Jiang, W. Huang, Catal. Lett. 125 (2008) 160–167.
[51] A. Penkova, K. Chakarova, O.H. Laguna, K. Hadjiivanov, F. Romero Saria, M.A. Centeno, J.A. Odriozola, Catal. Commun. 10 (2009) 1196–1202.
[52] O.H. Laguna, M.A. Centeno, F. Romero-Sarria, J.A. Odriozola, Catal. Today 172 (2011) 118–123.
[53] G. Balducci, J. Kaspar, P. Fornasiero, M. Graziani, M.S. Islam, J.D. Gale, J. Phys. Chem. B 101 (1997) 1750–1753.
[54] E. Mamontov, T. Egami, R. Brezny, M. Koranne, S. Tyagi, J. Phys. Chem. B 104 (2000) 11110–11116.
[55] S. Rossignol, F. Gérard, D. Mesnard, C. Kappenstein, D. Duprez, J. Mater. Chem. 13 (2003) 3017–3020.
[56] P. Vidmar, P. Fornasiero, J. KaÅ¡par, G. Gubitosa, M. Graziani, J. Catal. 171 (1997) 160–168.
[57] S. Carrettin, Y. Hao, V. Aguilar-Guerrero, B.C. Gates, S. Trasobares, J.J. Calvino, A. Corma, Chem.—Eur. J. 13 (2007) 7771–7779.
[58] H.T. Chen, J.G. Chang, H.L. Chen, S.P. Ju, J. Comput. Chem. 30 (2009) 2433–2442.
[59] Y. Liu, C. Wen, Y. Guo, G. Lu, Y. Wang, J. Phys. Chem. C 114 (2010) 9889–9897.
[60] W. Liu, A.F. Sarofim, M. Flytzani-Stephanopoulos, Appl. Catal. B 4 (1994) 167–186.
[61] J.Y. Ying, A. Tschöpe, Chem. Eng. J. 64 (1996) 225–237.
[62] D.R. Lite, CRC Handbook of Chemistry and Physics, New York, 2003-2004 25.